Magnetosheath for almost-aligned solar wind magnetic field and flow vectors: Wind observations across the dawnside magnetosheath at X = −12 Re

C. J. Farrugia,[1] N. V. Erkaev,[2,3] R. B. Torbert,[1] H. K. Biernat,[4,5] F. T. Gratton,[6] A. Szabo,[7] H. Kucharek,[1] H. Matsui,[1] R. P. Lin,[8,9] K. W. Ogilvie,[7] R. P. Lepping,[7] and C. W. Smith[1]

Received 23 November 2009; revised 24 March 2010; accepted 20 April 2010; published 27 August 2010.

[1] While there are many approximations describing the flow of the solar wind past the magnetosphere in the magnetosheath, the case of perfectly aligned (parallel or anti-parallel) interplanetary magnetic field (IMF) and solar wind flow vectors can be treated exactly in a magnetohydrodynamic (MHD) approach. In this work we examine a case of nearly-opposed (to within 15°) interplanetary field and flow vectors, which occurred on October 24–25, 2001 during passage of the last interplanetary coronal mass ejection in an ejecta merger. Interplanetary data are from the ACE spacecraft. Simultaneously Wind was crossing the near-Earth (X ~ −13 Re) geomagnetic tail and subsequently made an approximately 5-hour-long magnetosheath crossing close to the ecliptic plane (Z = −0.7 Re). Geomagnetic activity was returning steadily to quiet, "ground" conditions. We first compare the predictions of the Spreiter and Rizzi theory with the Wind magnetosheath observations and find fair agreement, in particular as regards the proportionality of the magnetic field strength and the product of the plasma density and bulk speed. We then carry out a small-perturbation analysis of the Spreiter and Rizzi solution to account for the small IMF components perpendicular to the flow vector. The resulting expression is compared to the time series of the observations and satisfactory agreement is obtained. We also present and discuss observations in the dawnside boundary layer of pulsed, high-speed (v ~ 600 km/s) flows exceeding the solar wind flow speeds. We examine various generating mechanisms and suggest that the most likely cause is a wave of frequency 3.2 mHz excited at the inner edge of the boundary layer by the Kelvin-Helmholtz instability.

Citation: Farrugia, C. J., et al. (2010), Magnetosheath for almost-aligned solar wind magnetic field and flow vectors: Wind observations across the dawnside magnetosheath at X = −12 Re, *J. Geophys. Res.*, *115*, A08227, doi:10.1029/2009JA015128.

1. Introduction

[2] The study of the flow of the solar wind past the magnetosphere is an important subject which has been treated in various approximations. Since the flow is magnetized, a simple gas dynamical approach is inadequate. A very successful treatment has been elaborated by Spreiter and co-workers [*Spreiter et al.*, 1966; *Spreiter and Alskne*, 1969; *Spreiter and Stahara*, 1980; see also *Siscoe*, 2002]. Called the Convected Gas Dynamic Model (CGDM), the technique involves first a solution of the gas dynamic problem to obtain the plasma parameters and the flow field, including the position of the bow shock. Subsequently, the magnetic field is obtained by appeal to the frozen-in condition ($\mathbf{E} + \mathbf{V} \times \mathbf{B} = 0$). This treatment accounts for many gross features of the flow, except near the magnetopause, where the intensified magnetic field strength starts to exert a back influence on the flow, violating the assumptions of the CGDM. This leads to the formation of a so-called "plasma depletion layer" (PDL) when the magnetopause may be treated as a tangential discontinuity. In this layer [*Lees*, 1964; *Zwan and Wolf*, 1976; *Erkaev*, 1988] the magnetic field strength increases while the density decreases, and the flow assumes a stagnation line pattern [*Sonnerup*, 1974; *Pudovkin and Semenov*, 1977].

[3] In the special case when the interplanetary field (IMF) and solar wind flow vectors are aligned (parallel or anti-

[1]Space Science Center and Department of Physics, University of New Hampshire, Durham, New Hampshire, USA.
[2]Institute for Computational Modeling, Russian Academy of Sciences, Krasnoyarsk, Russia.
[3]Siberian Federal University, Krasnoyarsk, Russia.
[4]Space Research Institute, Austrian Academy of Sciences, Graz, Austria.
[5]Institute for Theoretical Physics, University of Graz, Graz, Austria.
[6]Instituto de Física del Plasma, Consejo Nacional de Investigaciones Científicas y Técnicas, Buenos Aires, Argentina.
[7]Space Weather Laboratory, NASA Goddard Space Flight Center, Greenbelt, Maryland, USA.
[8]Physics Department and Space Sciences Laboratory, University of California, Berkeley, California, USA.
[9]School of Space Research, Kyung Hee University, Korea.

0148-0227/10/2009JA015128

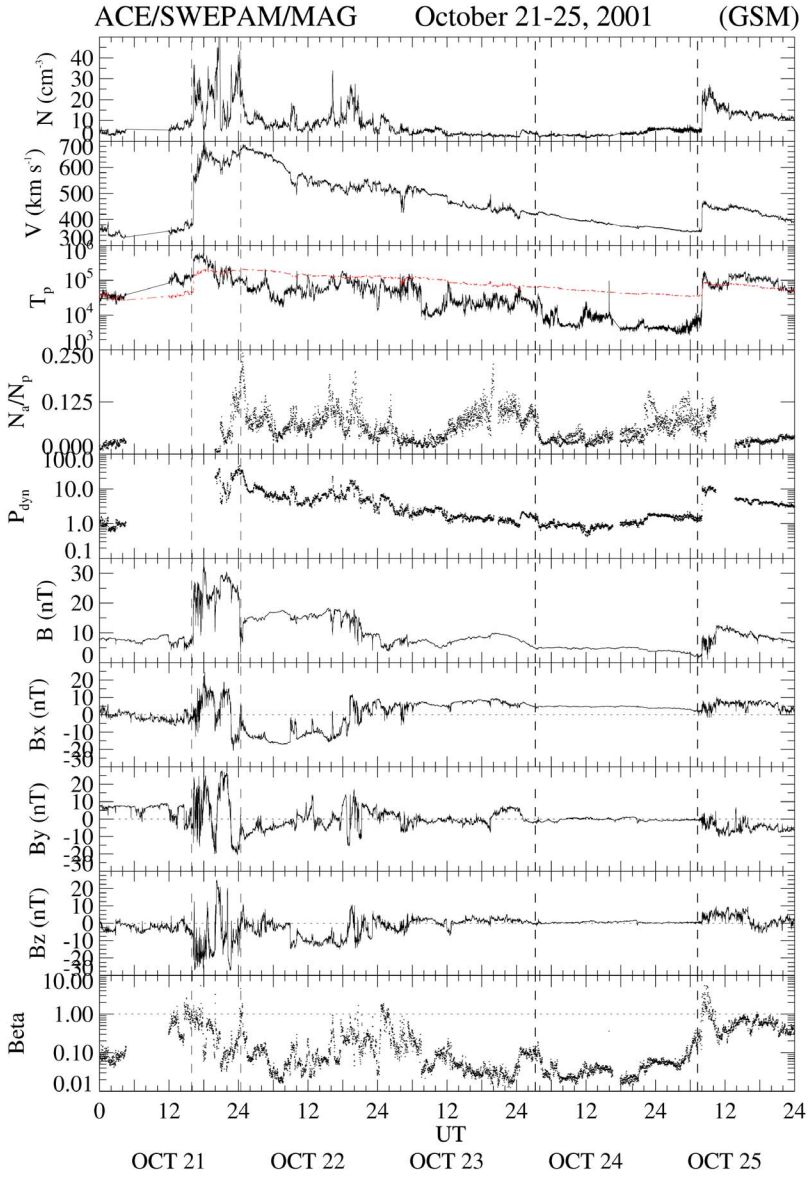

Figure 1. ACE observations in the 5-day period October 21–25, 2001. Shown are proton plasma density, bulk speed and temperature, the dynamic pressure, number density ratio of α particles to protons, the total field, and its GSM components, and the proton plasma beta.

parallel), however, a self-consistent, steady-state magnetohydrodynamic (MHD) solution was elaborated by *Spreiter and Rizzi* [1974]. In this case it is found that throughout the magnetosheath $\mathbf{B} \propto \rho\mathbf{V}$, where ρ is the mass density. Spreiter and Rizzi (SR) achieved this by constructing a pseudo gas with an unusual equation of state to which the MHD equations could be transformed. The magnetopause shape was computed from pressure balance conditions assuming a Newtonian equation for the pressure along the boundary (see below).

[4] Clearly, this situation (for most practical purposes, a radially-directed IMF) is a rare occurrence. However, it can sometimes be closely approached [e.g., see *Shue et al.*, 2009], as it did in the period we examine, October 24–25, 2001. Such a situation has great intrinsic physical interest. For example, one can carry out a perturbation analysis of the SR solution and compare with the data in the quasi-steady state limit. This is what we intend to do in this paper. In the magnetosheath pass we study, various time–dependent effects are seen in the data, not included in either theory. We discuss these briefly in the final section. In view of these, agreement between theory and observations is understood only in a time-averaged sense.

[5] The event we study is also interesting for a second reason. When inside the low latitude boundary layer, Wind observed repeated pulses of an accelerated plasma. We shall describe these and from their properties infer the most likely explanation.

[6] The layout of the paper is as follows. We first present the interplanetary data. Then we check the relation between the magnetosheath magnetic field and the product of the density and bulk velocity resulting from Wind measurements and compare them with the SR predictions. We then perform a perturbation analysis of the SR solution and

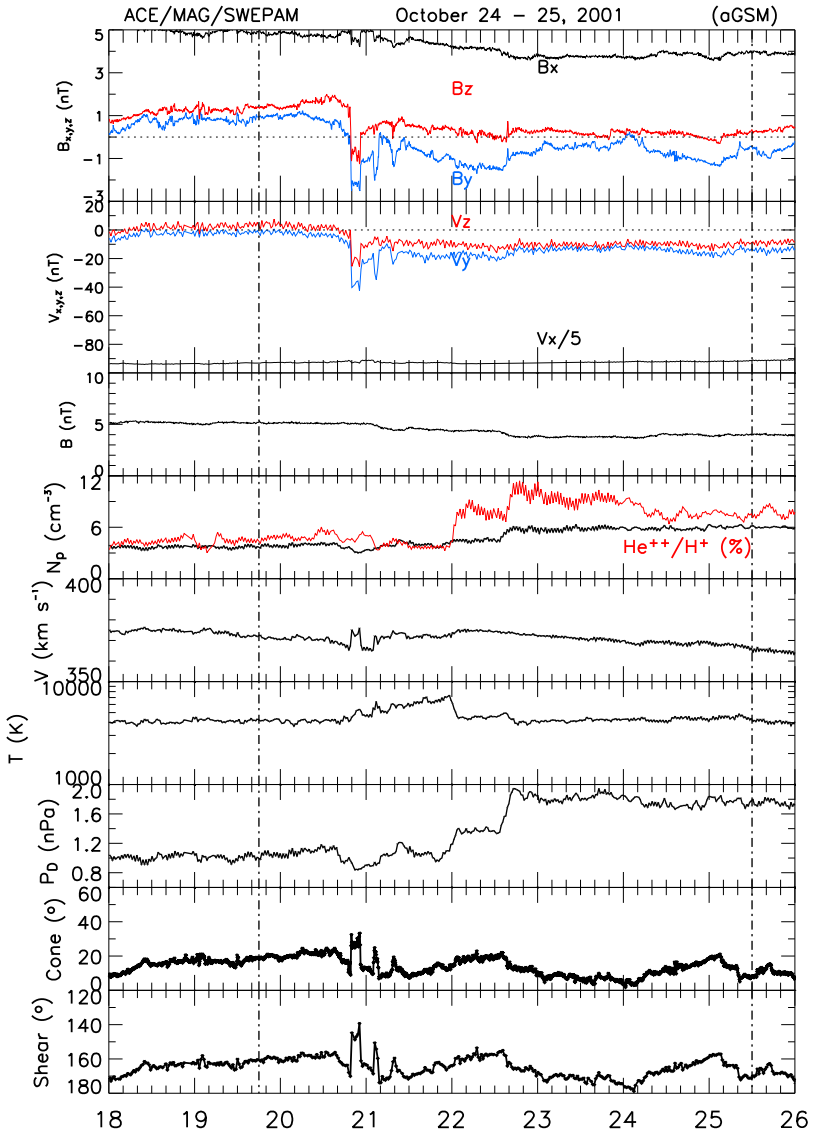

Figure 2. ACE Data for 18 UT (24)–2 UT (25). Shown are the (aberrated) GSM components of the magnetic and flow fields, the magnetic field strength, the density He^{++}/H^{+} in % (red), bulk speed and temperature, the dynamic pressure and the cone and shear angles. The interval between the vertical guidelines corresponds to near-Earth interplanetary values during Wind's magnetosheath traversal.

repeat and extend the comparison with Wind data. The earlier passage through the boundary layer is treated next. In the discussion we elaborate on the time-dependent features of the magnetosheath which go beyond the scope of steady MHD flow theories.

2. Interplanetary Observations

[7] Figure 1 gives an overview of ACE observations during the 5-day period October 21–25, 2001. The panels show from top to bottom the proton number density, bulk speed, and temperature, the α-particle - to - proton number density ratio, the dynamic pressure, including the contribution of the α-particles, the total magnetic field, and its GSM components, and the proton β. As described by *Farrugia et al.* [2007], the interplanetary configuration is that of an ejecta merger, where two or more interplanetary coronal mass ejections (ICMEs) meet on their way to Earth and (partly or totally) coalesce after the manner described by *Gopalswamy et al.* [2001] and *Burlaga et al.* [2002]. A strong shock driven by this ejecta merger (first vertical guideline) passes ACE at 16 UT (21). (Below we shall use for convenience the notation x UT (y) to mean x UT on day y in October 2001.) A shock-like feature is seen overtaking the ejecta merger at ~07:30 UT (25). Noteworthy are (i) the high N_α/N_p density ratios from October 22 until the time of arrival of this feature, reaching on occasion up to 25%; (ii) the low proton temperatures when compared with expected solar wind values (the latter after *Lopez* [1987]; red trace); (iii) the strong fields, at least in the earlier part of the merger; and (iv) a speed profile which over more than three days

Table 1. Parameter Values at ACE 19:45 UT on Oct 24 to 01:30 UT on Oct 25

Parameter	Unit	Value
N_p	[cm^{-3}]	4.93 ± 0.99
V_x	[km s^{-1}]	−370.37 ± 2.31
P_{dyn}	[nPa]	1.46 ± 0.39
B_z	[nT]	0.45 ± 0.58
$B_{\perp y}$	[nT]	−0.65 ± 0.83
V_p	[km/s]	370.80 ± 2.27
V_y	[km s^{-1}]	−13.67 ± 6.65
B_x	[nT]	4.16 ± 0.43
B	[nT]	4.31 ± 0.58
$B_{\perp z}$	[nT]	0.38 ± 0.63
T_p	[K]	4612.0 ± 741.9
V_z	[km s^{-1}]	−8.07 ± 5.43
B_y	[nT]	−0.50 ± 0.78
$B_{\perp x}$	[nT]	0.04 ± 0.05
Shear	[°]	164.6 ± 6.2

declines steadily from ~700 to ~350 km s^{-1}, a distinctive interplanetary feature of these mergers [*Burlaga et al.*, 2002]. This ejecta merger caused a double-dip major storm on October 21–22 (two Dst minima <−100 nT), which then subsided so that the magnetosphere was steadily returning to a quiet state during October 24–25 (between the last two guidelines; see *Farrugia et al.* [2007], where indices of geomagnetic activity are presented). Our interval of interest occurs during this quiet phase, and extends from 18 UT (24)–02 UT (25). One notes the very smooth and weak magnetic field, the cold solar wind plasma, the enhancement of α/p number density ratio later in the period, and the almost radial magnetic field direction. These are particularly "benign" interplanetary conditions.

[8] The interval 18 UT (24)–02 UT (25) is shown expanded in Figure 2. The panels show, from top to bottom, the magnetic field and flow velocity components, both in aberrated GSM coordinates, where one-fifth of V_x is shown for clarity, the total field strength, the proton density and, in red, the α particle - to - proton density ratio (%), the bulk speed, the temperature, the dynamic pressure including the alpha-particle contribution, the cone angle, i.e. the angle the IMF makes with the Sun-Earth line, and the "shear" angle, i.e. that between the magnetic field and plasma flow vectors. From the latter parameter it is seen that the field and flow vectors are approximately anti-parallel. A field and flow discontinuity occurs at 20:50 UT where the magnetic field turns briefly southward ($B_z \sim -1.2$ nT) and westward ($B_y \sim -2.8$ nT), after which B_y remains small and negative while B_z returns to small, positive values. Performing an average of various parameters on the subinterval 19:45 (24)–01:30 UT (25) (between the vertical guidelines), which we shall need when discussing Wind's magnetosheath observations, we have the values shown in Table 1 (as mean and standard deviation). During this interval the shear and cone angles are 164.65 ± 6.16° and 13.82 ± 5.70°.

[9] Figure 3 shows various derived quantities from ACE, namely, the sound, Alfvén, magnetosonic, and bulk flow speeds and the sonic, Alfvén-Mach, and magnetosonic-Mach numbers and, lastly, the proton plasma beta. While solar ejecta have typically an Alfvén Mach number of 2–4 [*Farrugia et al.*, 1995], here the Alfvén Mach number is not so small (≥6). This will be important for later considerations.

3. Magnetosheath Observations by Wind

[10] The GSE coordinates of the orbit of the Wind spacecraft in the interval 08 UT (24)–08 UT (25) are shown in Figure 4. The spacecraft advances dawnward (increasingly negative y-coordinate) from the central geomagnetic tail, passing through the near-equatorial boundary layer ("LLBL") and magnetosheath ("Msheath") before entering into the solar wind. The magnetosheath crossing is shown in red. It takes place close to the ecliptic plane (Z < 1 Re), at an average X-distance = −13.2 ± 0.39 Re. The magnetosheath is entered at Y = −25 Re and the solar wind at Y = −30.5 Re.

[11] The shape of the model magnetopause is shown in Figure 5. It is based on the *Shue et al.* [1998] model using values of the interplanetary B_z and dynamic pressure measured by ACE when Wind is crossing into the magnetosheath. The use of the Shue et al. model magnetopause requires some explanation. This model uses as input the IMF B_z component and the solar wind dynamic pressure and does not include the angle between the solar wind flow vector and the IMF. As one can see, it does not predict the position of Wind (i.e. at the magnetopause) well. A study was undertaken by *Merka et al.* [2003], comparing two-spacecraft observations of bow shock and magnetopause crossings with various models of these boundaries. The study was for almost antiparallel flow and field vectors upstream of the bow shock. They use the Shue et al. model for the magnetopause shape and they, too, find that it does not predict the intersections of the spacecraft with the magnetopause well. However, they find that agreement is much better if they increase the model subsolar distance by 20%. If we were to do this to our case and push the subsolar magnetopause outward by this amount (from 11.4 to 13.7 Re) and if we were then to draw a self-similar shape for the magnetopause surface away from the subsolar point, we would obtain much better agreement with Wind's location. The flaring of the magnetopause at Wind's location is ~15°. From their two-point measurements, *Merka et al.* [2003, Figure 10] suggest a model magnetopause ("bullet shape") with a flaring at the flanks which appears visually to be somewhat less than this, but there are some uncertainties in their derivation. Below we shall use the *Shue et al.* [1998] shape, with a flaring angle of 15°, and also report calculations when we arbitrarily reduce the flaring angle to 10°.

[12] Figure 6 shows the omni-directional differential energy fluxes for electrons in the energy range 10–1000 eV from the 3 Dimensional Plasma Analyzer on Wind [*Lin et al.*, 1995]. It shows clearly the passage from the magnetosphere (left, high energies) to the solar wind (right, low energies). From 19–20:30 UT (24), there occur repeated incursions of high energy plasma. This is part of the structure of the LLBL that we discuss in section 5. The magnetosheath traversal takes place between ~20:40 UT (24) and 2:30 UT (25). During the early part of this, quasi-periodic modulations in the intensity of the low-energy electron component are visible, particularly from 21:15–22:30 UT (24). These are related to episodes of a cold and dense proton plasma soon after magnetosheath entry, as

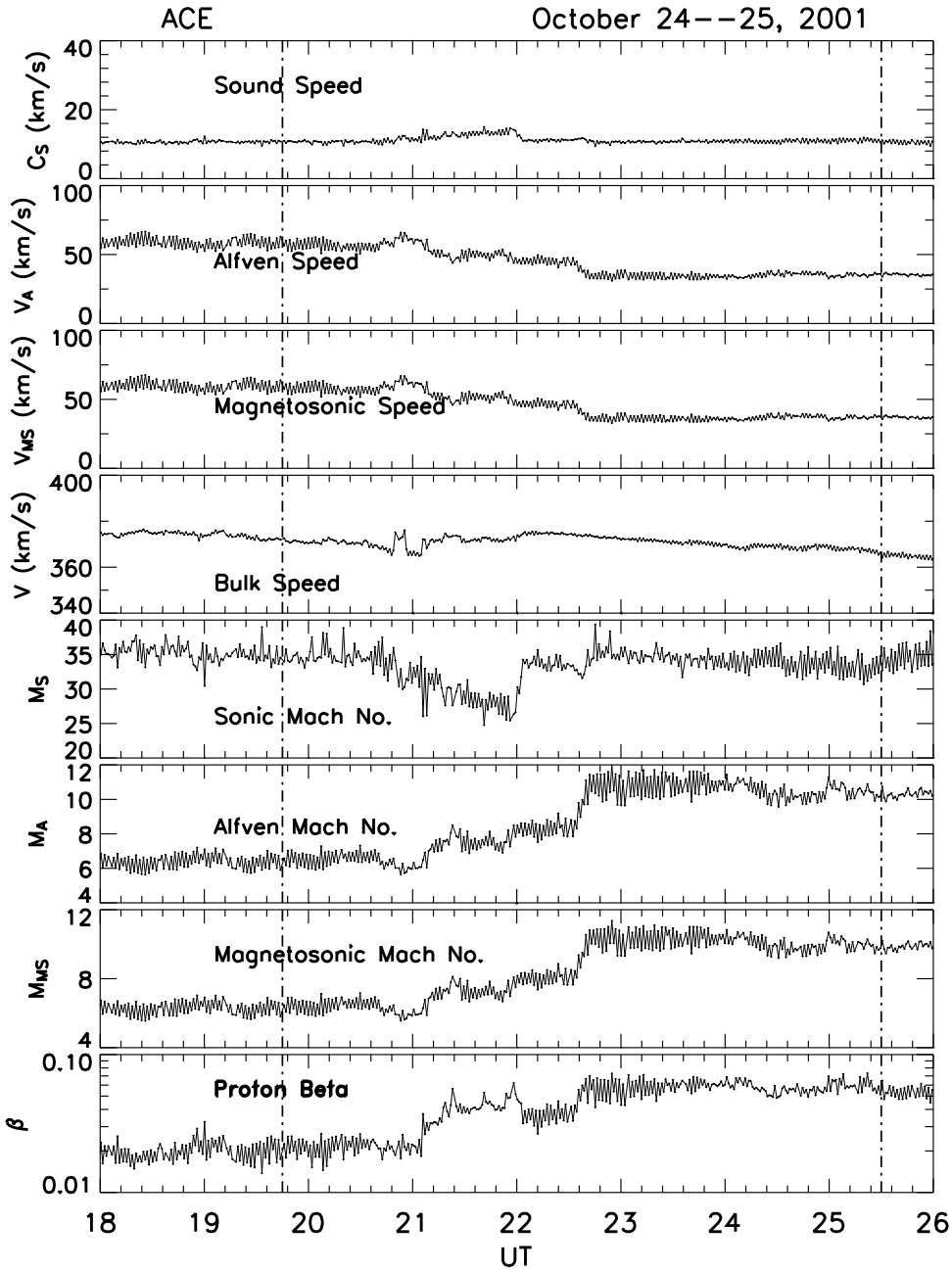

Figure 3. Various derived parameters from ACE for 18 UT (24)–2 Ut (25): sound, Alfén, magnetosonic and bulk speeds and the sonic-Mach, Alfvén-Mach and magnetosonic-Mach numbers, and the proton plasma beta.

detailed in Figure 7. Nowhere is the magnetosphere crossed, however.

[13] Figure 7 shows WIND observations from 20 UT (24) to 10 UT (25) including all the magnetosheath crossing and some part of the solar wind. The data are from the MFI [*Lepping et al.*, 1995] and the 3D plasma Analyzer [*Lin et al.*, 1995]. The data have been rotated to take account of the solar wind aberration in the flow direction. The temporal resolution for both data sets is 3 s but we have made a 5-point smoothing to diminish the fluctuations. From top to bottom, the panels give the proton density, bulk speed, temperature, magnetic field strength, and (pairwise) the field and flow components in GSM coordinates, and finally the sum of the thermal and magnetic pressures. The first vertical guideline marks the estimated time of the outbound magnetopause crossing (20:40 UT), before which the plasma was of very low density and high temperatures. The second vertical line at 02:30 UT (25) marks the first bow shock crossing followed by entry into the solar wind. There follows a period of 1.5 hours when there are repeated episodes of high density-low temperature plasma alternating with low density-high temperature plasma, and other changes in the parameters. These we believe to be repeated crossings of the bow shock.

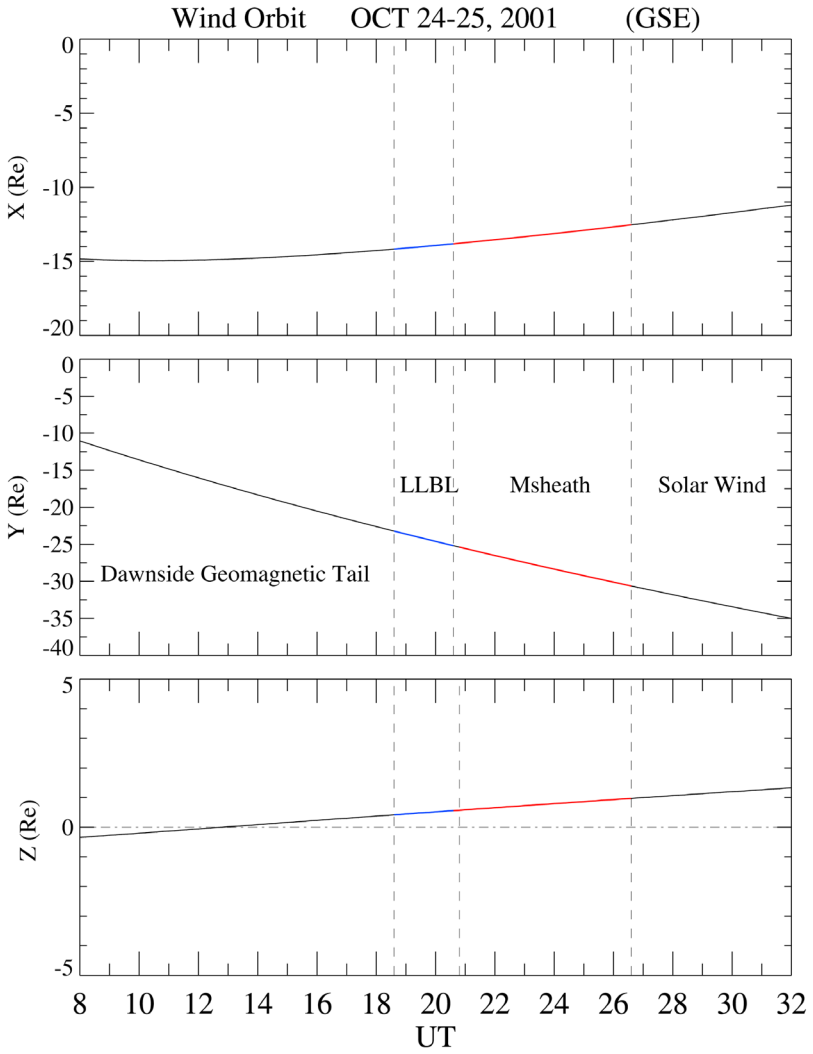

Figure 4. The GSE coordinates of spacecraft Wind from 08 UT (24)–08 UT (25). Regions crossed by the spacecraft are marked.

To diminish errors, these will not be included later when we perform analysis on the magnetosheath data.

[14] The red traces refer to ACE measurements in the solar wind delayed by 1 hour. Figure 7 shows that when Wind exits into the solar wind it encounters the shock-like feature mentioned above at the same time as ACE. The delay time of 1 hr is thus good to relate the two observations in the solar wind. When Wind is crossing the magnetosheath earlier, we need in principle to add a further delay of order 10 min for the shocked solar wind to propagate through the magnetosheath and arrive at Wind. The exact value is hard to estimate but in our case not necessary since conditions in the solar wind are quasi-steady.

[15] Clearly, in the magnetosheath observations there is temporal variability, which may be of different origins. For example, there are three instances of low temperature-high density proton plasma from 21:15–22:30 UT, also noted in connection with the electron differential energy fluxes in Figure 6. We defer a discussion of these until later. We shall concentrate next on the average, steady aspects using a one-fluid MHD approach.

4. Field and Flow Relations in the Magnetosheath

4.1. Exactly Aligned Magnetic and Flow Fields

[16] The basic result of the SR work (obtained also by *Imai* [1960] for continuous flows) is the equation

$$\mathbf{B} = \left(\frac{\mathbf{B}_\infty \cdot \mathbf{V}_\infty}{\rho_\infty V_\infty^2}\right)\rho\mathbf{V}. \qquad (1)$$

expressing a proportionality between magnetosheath quantities **B** and $\rho\mathbf{V}$. Taking average values from Table 1, the constant of proportionality is numerically equal to −0.0023. We can first make an approximation. From Figure 7 it emerges that the flow speed in the magnetosheath is roughly constant (V = 313.6 ± 15.7 km s^{-1}). We can then take absolute values of equation (1) and obtain that, according to SR, $B \propto N$, i.e. a linear relation with a slope of 0.74.

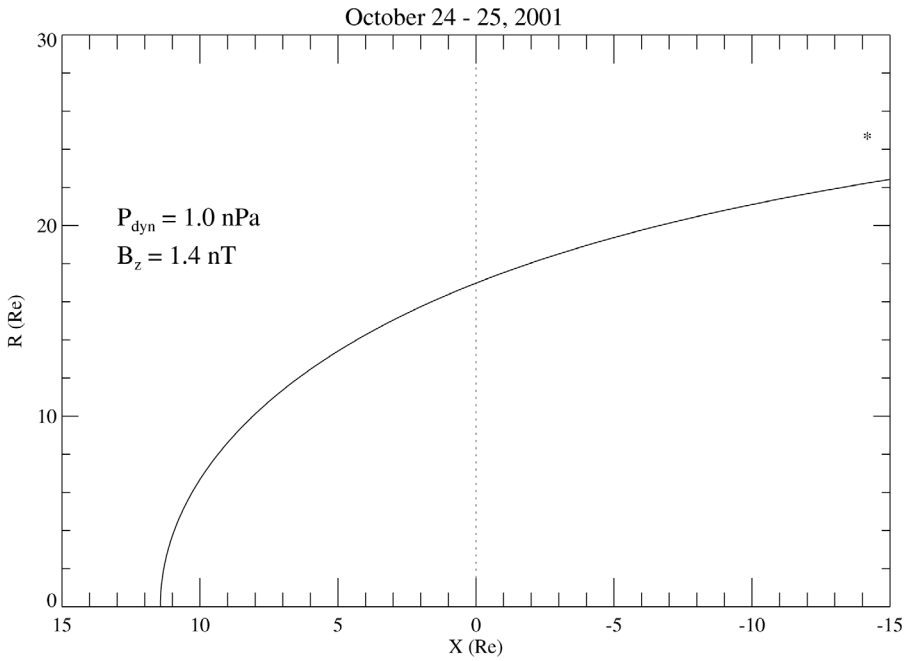

Figure 5. Model magnetopause after *Shue et al.* [1998] for a dynamic pressure of 1.0 nPa and an IMF B_z of 1.4 nT, corresponding to ACE values at the time when Wind is crossing into the magnetosheath (α-particles included).

Figure 8 plots B versus the proton density, N. Clearly, B and N are positively correlated, the correlation coefficient being 0.53. With 6484 data points, this implies a correlation at more than the 99.9% confidence level. The black straight line shows the predicted relation. The line of regression is shown in red. This deviates somewhat from that predicted: it has a steeper slope (= 0.95) and there is an offset. We note that plotting B versus $N_p \cdot V_p$ gives practically the same result.

[17] We next consider the components. The three panels of Figure 9 show scatter plots of the components of the magnetosheath magnetic field versus the corresponding components of the velocity multiplied by the proton density. All three quantities are anti-correlated and the best correlation occurs for the major component, X. The correlation coefficients are −0.55 (X), −0.23 (Y) and −0.33 (Z) The regression lines are drawn in red. The black lines now give the SR-theoretical values (see equation 1), where we have used the average value for the proportionality constant from Table 1 (i.e. $B_{x,\infty}/(\rho_\infty V_\infty)$). It is seen that the agreement is quite good except for B_z. This is the component which is affected most by the perturbation of the IMF (i.e. the departure from strict antiparallel solar wind magnetic and flow fields). This is because, while V_y in the solar wind is as

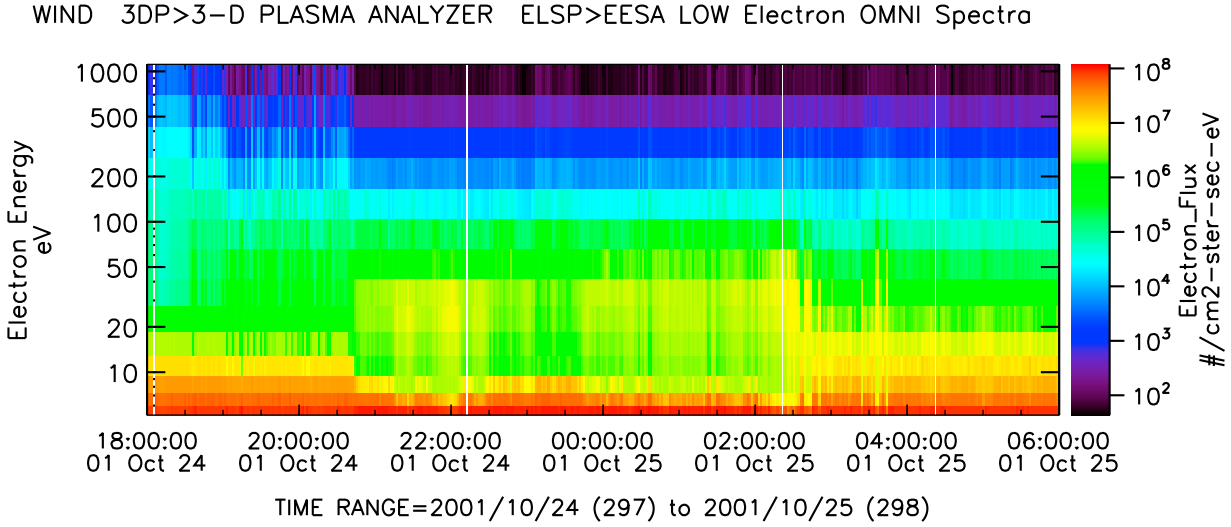

Figure 6. Electron differential energy flux as a function of time-varying energy in the range 5–1200 eV from the 3D Plasma Analyzer on Wind.

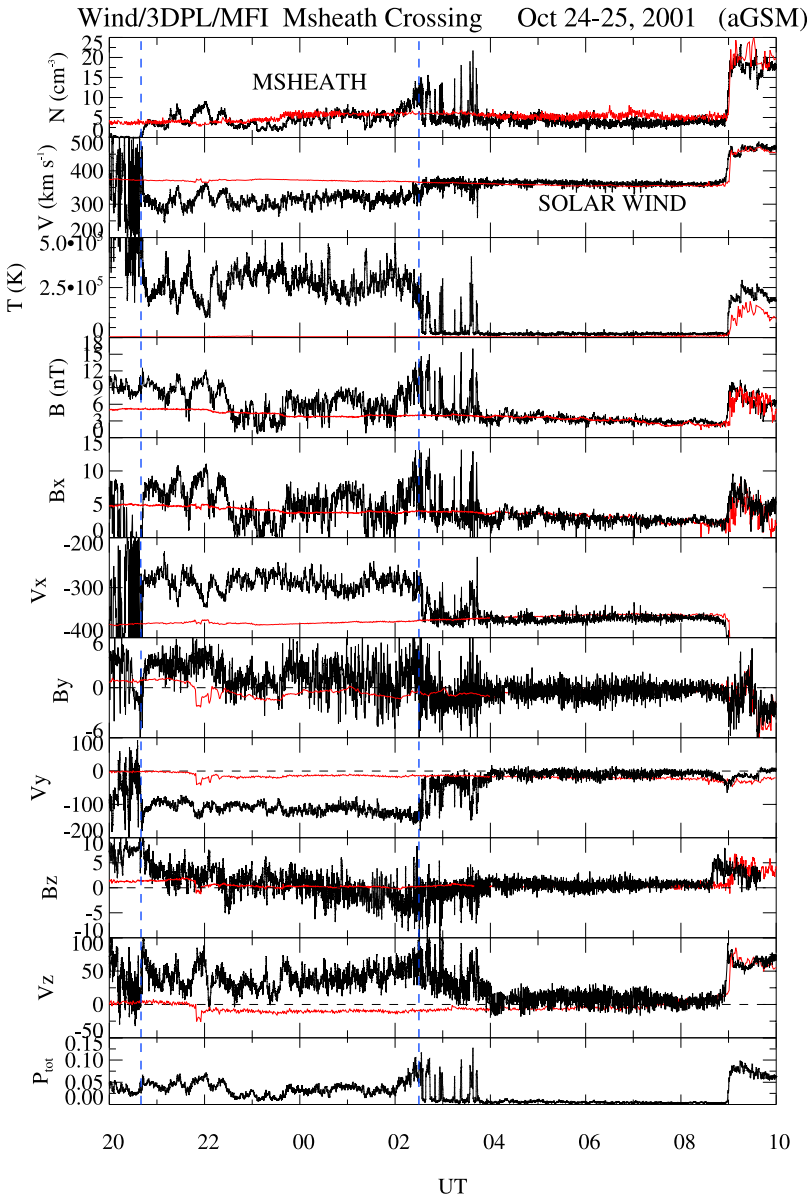

Figure 7. Wind observations in the magnetosheath (between the blue vertical guidelines) and in the solar wind. Shown are the proton density, bulk speed and temperature, he total field, (pairwise) components of the magnetic and flow fields and the total pressure. For further details, see text.

small as V_z (see Figure 2), the flaring of the magnetopause (Figure 5) leads to a substantial V_y in the magnetosheath, but little in V_z since the Wind measurements are being made near the ecliptic plane.

[18] We now perturb this solution to take account of the small deviations from strictly anti-parallel directions.

4.2. Almost-Aligned Magnetic and Flow Fields

[19] Using the solution of *Spreiter and Rizzi* [1974] as background, we introduce a perturbation in magnetic field components in the magnetosheath, $\delta\mathbf{B}$

$$\mathbf{B} = -\frac{B_{x\infty}}{\rho_\infty V_\infty}\rho\mathbf{V} + \delta\mathbf{B}. \tag{2}$$

[20] The magnetic field components in a curvilinear coordinate system fixed to the magnetopause are determined by the formulae derived in Appendix A, i.e.,

$$B_l = [B_{z\infty}\cos(\phi) + B_{y\infty}\sin(\phi)]\sqrt{2\psi(\mu,r)}\frac{1}{a_0\tilde{r}\mu} - B_{x\infty}\tilde{\rho}\tilde{V}_l, \tag{3}$$

$$B_\phi = [-B_{z\infty}\sin(\phi) + B_{y\infty}\cos(\phi)]\frac{\tilde{r}\tilde{\rho}}{\sqrt{2\psi(\mu,r)}}, \tag{4}$$

$$B_\mu = [B_{z\infty}\cos(\phi) + B_{y\infty}\sin(\phi)]\sqrt{2\psi(\mu,\tilde{r})} \cdot\frac{(a_0 - a)}{a_0\tilde{r}\tilde{V}_l(\tilde{r})} - B_{x\infty}\tilde{\rho}\tilde{V}_\mu, \tag{5}$$

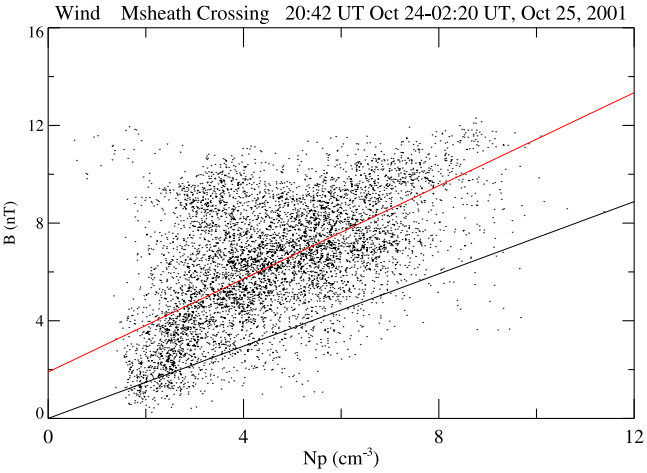

Figure 8. The magnetosheath magnetic field strength plotted against the proton density. The red line is the regression line. The black line is the one derived from the Spreiter-Rizzi equation (1) with a constant of proportionality $\langle V\rangle B_{x\infty}/n_\infty V_\infty$. Here $\langle V\rangle$ is the average speed in the magnetosheath and the other quantities are obtained from the Table 1.

where μ is the distance perpendicular to the magnetopause, normalized to R_0, the subsolar distance of the magnetopause, l is a length along the magnetopause (meridional), and ϕ is the azimuthal angle. The origin of the coordinate system (μ, l, ϕ) is the stagnation point. Quantity ψ is the stream function, which is related to the plasma velocity components by

$$\frac{\partial\psi}{\partial\mu} = \tilde{\rho}\tilde{V}_l\tilde{r}, \tag{6}$$

B_l, B_ϕ, and B_μ are the meridional, azimuthal and normal magnetic field components with respect to the magnetopause, $\tilde{\rho}$ is the dimensionless plasma density (normalized to ρ_∞), $\tilde{V}_l$ and $\tilde{V}_\mu$ are the dimensionless meridional and normal velocity components (in units of V_∞), $\tilde{r}$ is the dimensionless cylindrical radius (a distance from the axis of symmetry normalized to the subsolar distance R_0). The dimensionless parameter a is defined as the derivative of the normal velocity component in the direction orthogonal to the magnetopause.

$$a = \left|\frac{\partial\tilde{V}_\mu}{\partial\mu}\right|. \tag{7}$$

The parameter a_0 is defined as the value of a referred to the stagnation point.

$$a_0 = a(0). \tag{8}$$

When we approach the magnetopause, the stream function decreases to zero, and thus the perturbations of the magnetic field components increase.

[21] Analytical formulae for the quantities $\tilde{\rho}$, $\tilde{V}_{l,\mu}$ and a are given in Appendix B, where we specifically use the shape of the magnetopause given in Figure 5.

[22] The Wind trajectory through the magnetosheath in the interval 20:40 UT (24)–02:30 UT (25) is mainly in the Y direction (Figure 4). Applying formulas (2)–(5) for this case, we find the following magnetic field components along the satellite trajectory.

$$B_x = B_{y\infty}\sqrt{2\psi(\mu,r)}\frac{1}{a_0\tilde{r}\mu}\sin(\theta) + B_{x\infty}\tilde{\rho}\tilde{V}_l\sin(\theta), \tag{9}$$

$$B_z = B_{z\infty}\frac{\tilde{r}\tilde{\rho}}{\sqrt{2\psi(\mu,r)}}, \tag{10}$$

$$B_y = B_{y\infty}\sqrt{2\psi(\mu,r)}\frac{(a_0-a)}{a_0\tilde{r}\tilde{V}_l(r)}\sin(\theta) + B_{x\infty}\tilde{\rho}\tilde{V}_\mu\sin(\theta) + B_{y\infty}\sqrt{2\psi(\mu,r)}\frac{1}{a_0\tilde{r}\mu}\cos(\theta) + B_{x\infty}\tilde{\rho}\tilde{V}_l\cos(\theta). \tag{11}$$

Here θ is the angle between the outward normal to the magnetopause and the GSM X axis. The normal distance μ is determined as a linear function of time during Wind's passage through the magnetosheath, i.e. we transform times into distances as follows:

$$\mu = c_1(t - t_0), \tag{12}$$

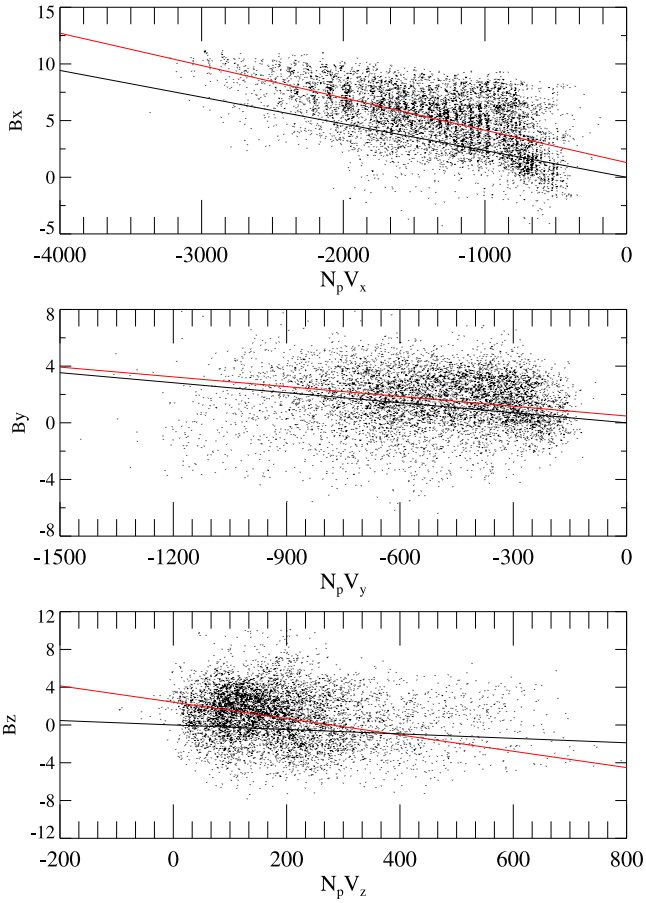

Figure 9. A comparison of the SR relation component by component from data during Wind's magnetosheath traversal. The black lines are the predictions of the SR theory, and the red lines are the fitted regression lines.

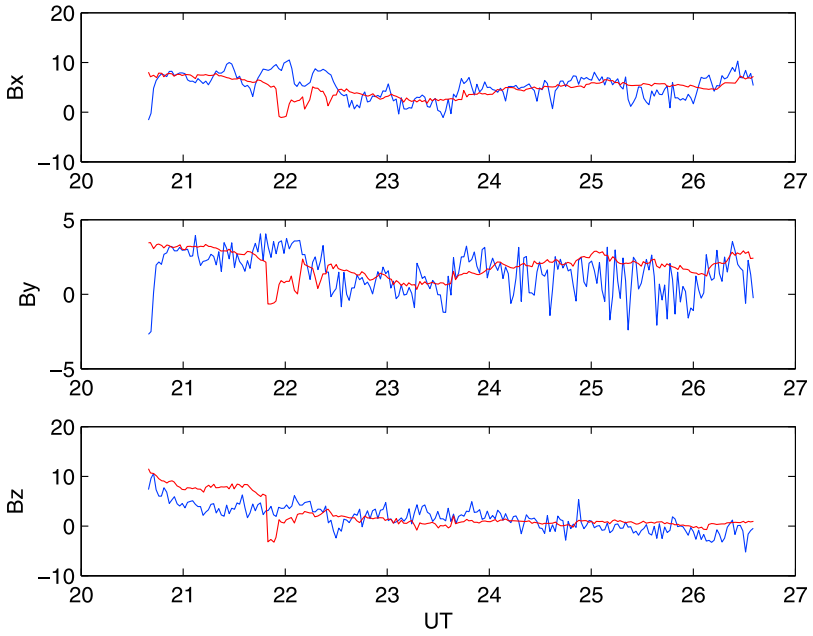

Figure 10. The theoretical MHD field components of the perturbed Spreiter-Rizzi theory (red traces) are plotted as a function of time. The corresponding Wind observations are shown in blue.

where t_0 is the time corresponding to the magnetopause crossing ($t_0 \simeq$ 20:40 UT (24)). The IMF components $B_{x,y,z,\infty}$ are taken from ACE data with time delay $\tau \sim 1$ hour

$$B_{x,y,z,\infty} = B_{x,y,z,\infty}(t - \tau). \tag{13}$$

[23] In Figure 10 these theoretical quantities are plotted componentwise as a function of time (red traces) together with the measured values (blue traces). There is generally a good agreement between the theory and the data in all components. Recall that the theory is quasi steady-state so that rapid temporal variations will not be reproduced well. A clear example of these is in the period around 1–2 UT (25). The high frequency fluctuations are likely produced by internal instabilities [e.g., see *Anderson*, 1995]. There is also some disagreement around the time when the delayed field at ACE has a sharp southward turning (~22 UT; see Figure 2). This occurs during the ~1-hr period of large-amplitude, correlated changes in B, B_x and N around 22 UT (24) soon

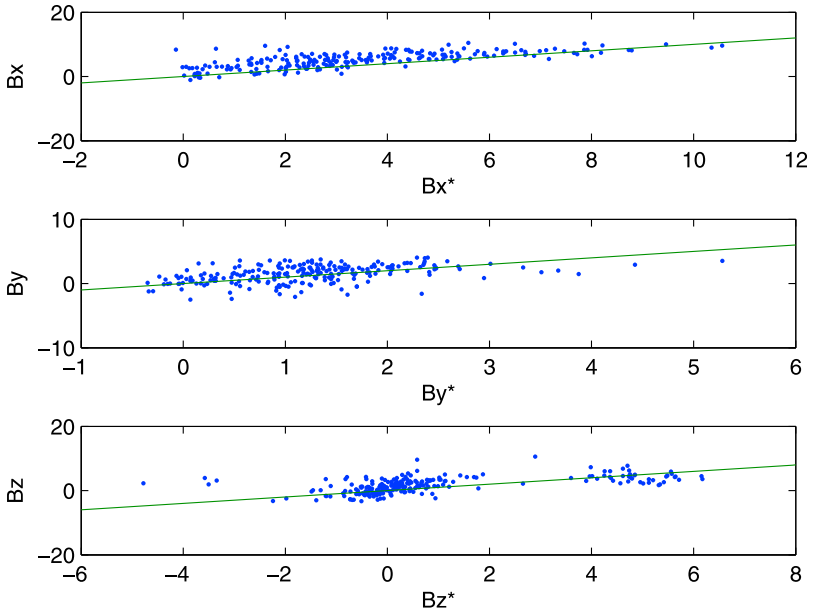

Figure 11. The observed magnetic field components (Y-axes) are plotted against the corresponding results from the perturbed SR theory. The green lines represents complete agreement between the theory and the data.

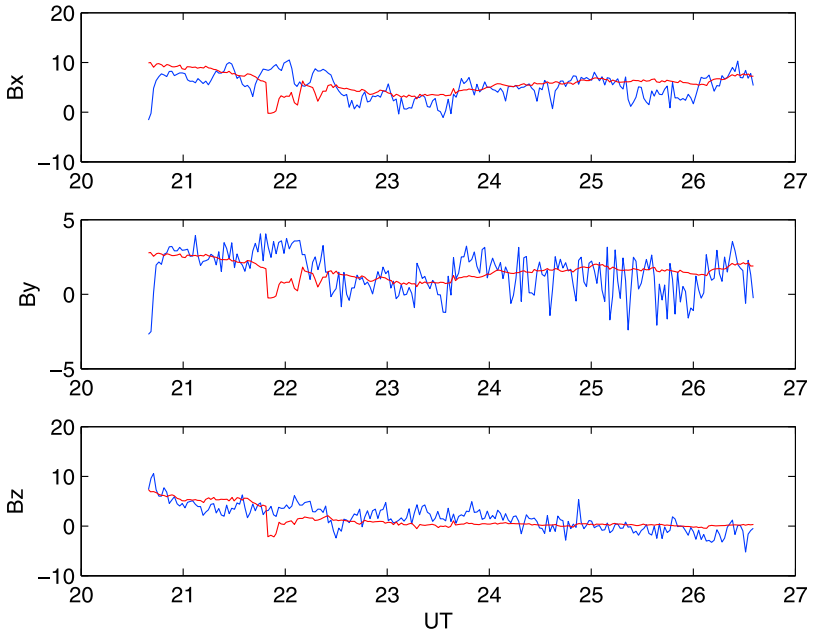

Figure 12. Similar to Figure 10 but for a flaring angle at Wind's location of 10°.

after Wind's exit into the magnetosheath (see Figure 7). As noted earlier, these oscillations are related to modulations of electron differential energy fluxes discussed above in connection with Figure 6. The cause of this is at present unclear.

[24] In Figure 11 we plot the observed magnetic field components versus the magnetic field calculated from equations (9)–(11), which include the SR theory corrected for a small perturbation. In these formulae we have normalized the magnetosheath density and velocity taken from Wind observations by their values in the interplanetary medium, the latter being averages as before (Table 1). If all points were to lie on each of the straight diagonal lines, the perturbed theory would account for the data completely. As one can see, the trends are reproduced very well. However, the steady-state theory tends to underestimate the data, particularly in the B_x component. This, we believe, is a reflection of temporal changes not included in any quasi-steady state treatment.

[25] Figure 12 presents plots for B_x, B_y, and B_z along Wind's trajectory when the magnetopause flaring is reduced from 15° to 10°. Comparison with Figure 10 shows that this variation does not make have a significant influence on the magnetic field components along the Wind trajectory. The two plots are nearly identical in the inner magnetosheath. However, some small differences can be seen in vicinity of the magnetopause. In the second case (for a flaring of 10°), the B_x component is somewhat larger, and the B_y and B_z components are slightly smaller, than those in the first case.

5. Pulsed Accelerated Flows in the Equatorial Boundary Layer at Dawn

[26] We now describe Wind observations during its transit through the dawnside LLBL from ~19 UT to 20:30 UT, October 24. Figure 13 shows the time series of various physical quantities in this interval: proton plasma density, bulk speed, temperature, total field and its GSM components, and the flow field, also in GSM coordinates. Figure 14 shows a shorter, 30 min interval for clarity. A prominent feature of the observations is the pulsed behavior in most parameter values. In each pulse, the total flow velocity increases up to, and even exceeds at times 600 km s^{-1} (i.e. much higher than the solar wind speed which was of order 400 km s^{-1}). The density increases but, typically, not synchronous with velocity increase but rather rises when the velocity has dropped to background values. Sometimes density enhancements are absent or weak (see for example the period 19:35–20 UT). The enhanced bursts of dense plasma are typically cold, i.e., it is a cold dense plasma typical of the magnetosheath. Each pulse is accompanied by large changes in all flow components where, in particular, the V_x becomes more negative (i.e. increases anti-sunward). In each pulse, the field components B_x and B_y undergo a polarity reversal from positive to negative. By contrast, the B_z component increases but remains positive. A remarkable feature of the observations is their strict periodicity. If we time the period by the minima in B_y we obtain a value of 5.15 ± 1.09 min, i.e. of average frequency ~3.2 mHz.

[27] In view of these properties we conjecture that these perturbations are waves in the boundary layer. Wind enters each of these where the accelerated plasma results from the sum of the magnetosheath velocity and the phase velocity of the wave. The instances of high density and cold plasma represent brief entries into magnetosheath as the wave passes by. The waves may have been generated by the Kelvin-Helmholtz (KH) instability acting at the inner edge of the LLBL. At the magnetopause, at least locally, the magnetic shear (60.7° and 50.0° using averages over 20 and 10 min intervals on either side of the magnetopause, respectively) is too large not to inhibit their growth. At the inner edge of the LLBL we obtain a field shear of 3.8° and 2.0° for averages over 20 and 10 min, respectively. The

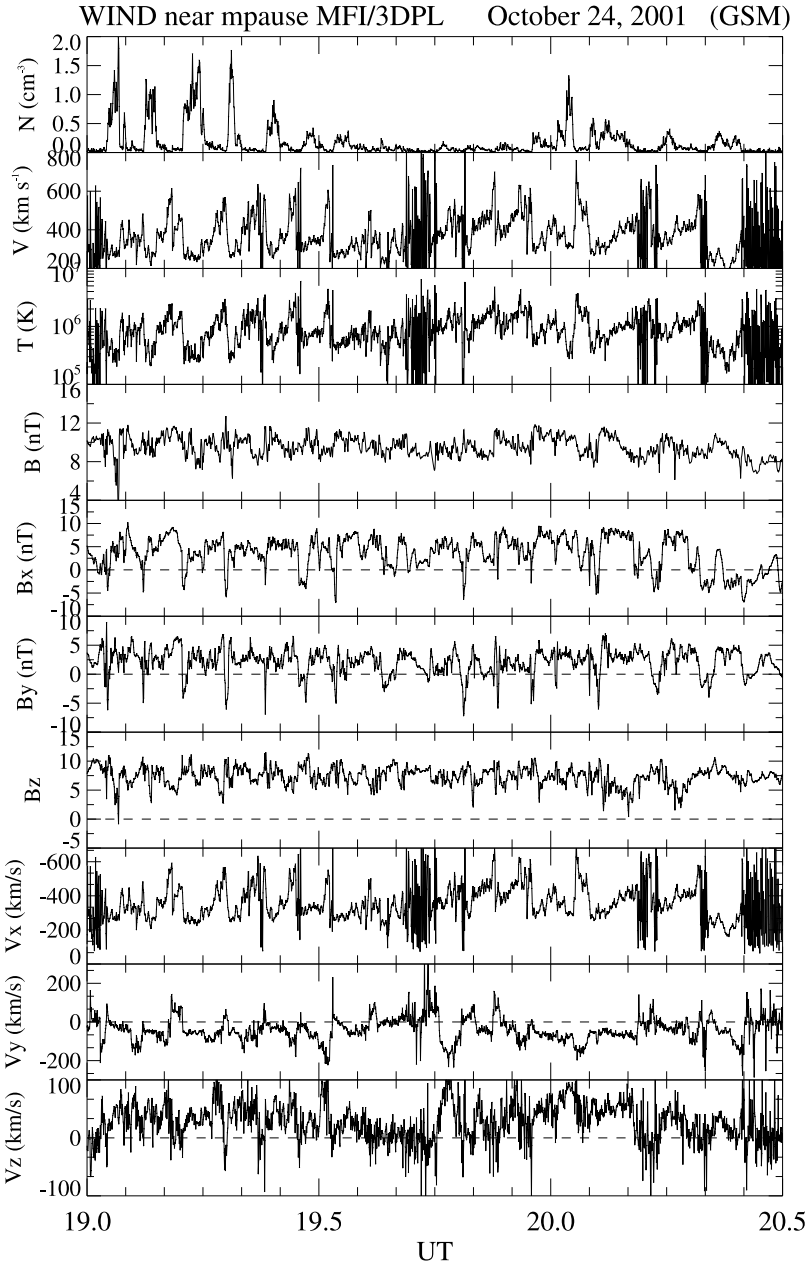

Figure 13. Pulsed field and flow behavior and accelerated flows in the LLBL.

fields at the inner edge of the LLBL are thus aligned, allowing the growth of KH waves.

[28] Other possible explanations, detailed in section 6 seem to us less plausible.

6. Discussion and Conclusions

[29] We have examined a crossing of the near - equatorial dawnside magnetosheath made by the Wind spacecraft on October 24–25, 2001 under conditions when the IMF was almost anti-parallel to the solar wind velocity (to within ~15°). This orbit was particularly good since it allows us to examine a dawnside cut of the magnetosheath near the ecliptic plane at a practically constant downtail distance. The solar wind was also generally quiet and the magnetosphere was recovering steadily from earlier activity [see *Farrugia et al.*, 2007, Figure 2]. We then applied the Spreiter and Rizzi self-consistent MHD flow theory to the measurements and found good agreement with predictions. Clearly, an implicit assumption in the use of equation (1) is that the derived moments from ACE and Wind observations have no significant instrumental uncertainties. Further, we undertook a perturbation analysis, adding small components of the IMF perpendicular to the flow vector. This constitutes, in our view, a substantial advance in the study of solar wind flow around the magnetosphere. A further factor is that the interaction of the solar wind, in which is embedded a quasi-radial IMF, with the magnetosphere has

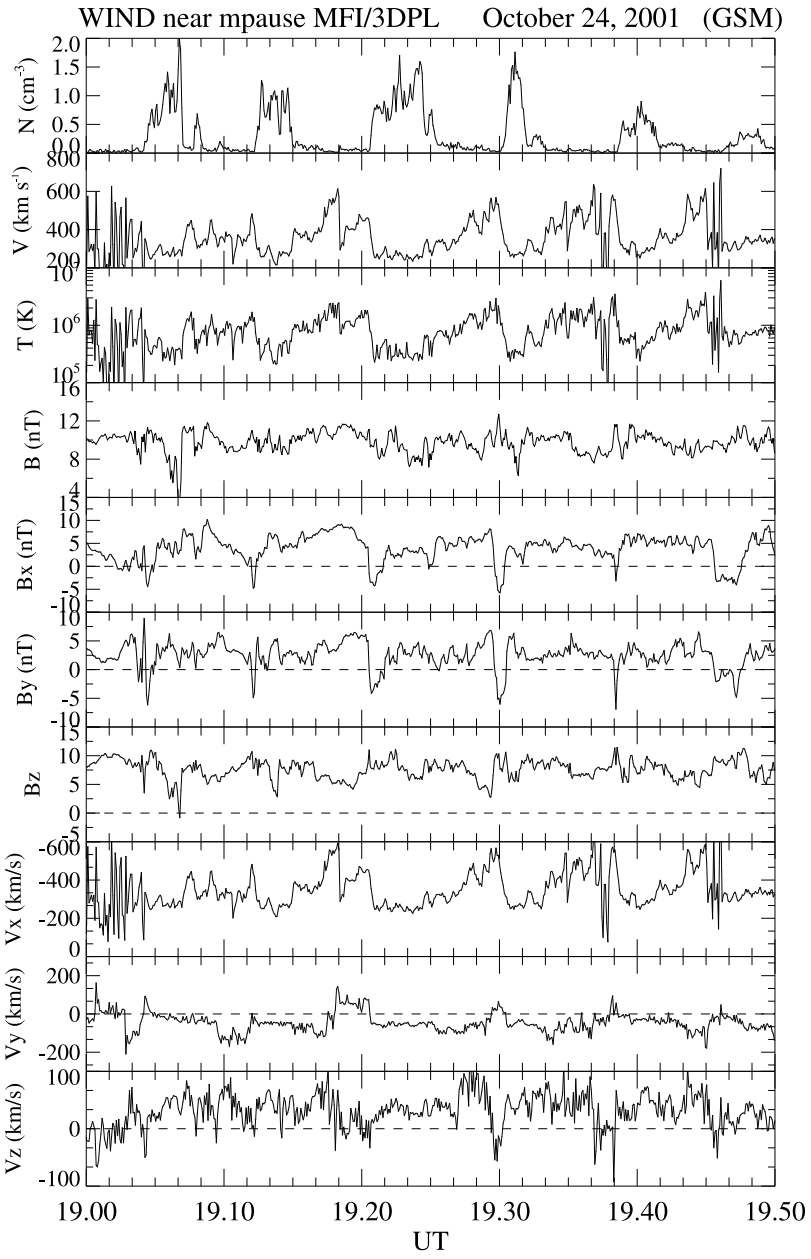

Figure 14. A 30-min close-up view of the pulsed behavior in the boundary layer.

been given only scant attention in the literature. When compared to the observations, this perturbed theory resulted in good agreement, although there were some discrepancies which we ascribe to temporal variations and inherent instabilities.

[30] Ours (and SR's) is a one-fluid theory. In this respect some discrepancies are to be expected from the fact that the interplanetary medium is an ICME and has a non-negligible He^{++} population. The α particles typically have a differential speed with respect to the protons [e.g., see *Steinberg et al.*, 1996], and the value of this quantity in the interplanetary medium is not available to us.

[31] Our theory, and that of SR, is a quasi-steady state theory. Other discrepancies between theory and observations will also arise if there are temporal variations. This was the case in the example we studied. One of these occurred on exit into the magnetosheath where Wind saw a modulation of low-energy electron fluxes and correlated changes in B_x and B and N_p (around 22 UT (24)). This "breathing mode" of the magnetosphere would generally be ascribed to slowly-varying dynamic pressure changes. There were indeed slow changes in the dynamic pressure when the α-particle contribution is taken into account. But the correspondence in time is not very good.

[32] Another source of disagreement is the higher-frequency magnetosheath fluctuations. These are likely to be due to inherent instabilities, to which the magnetosheath is prone [e.g., see *Anderson*, 1995, and references therein]. Another explanation might be turbulence [e.g., *Sahraoui et al.*, 2006], but this is beyond the scope of this paper to

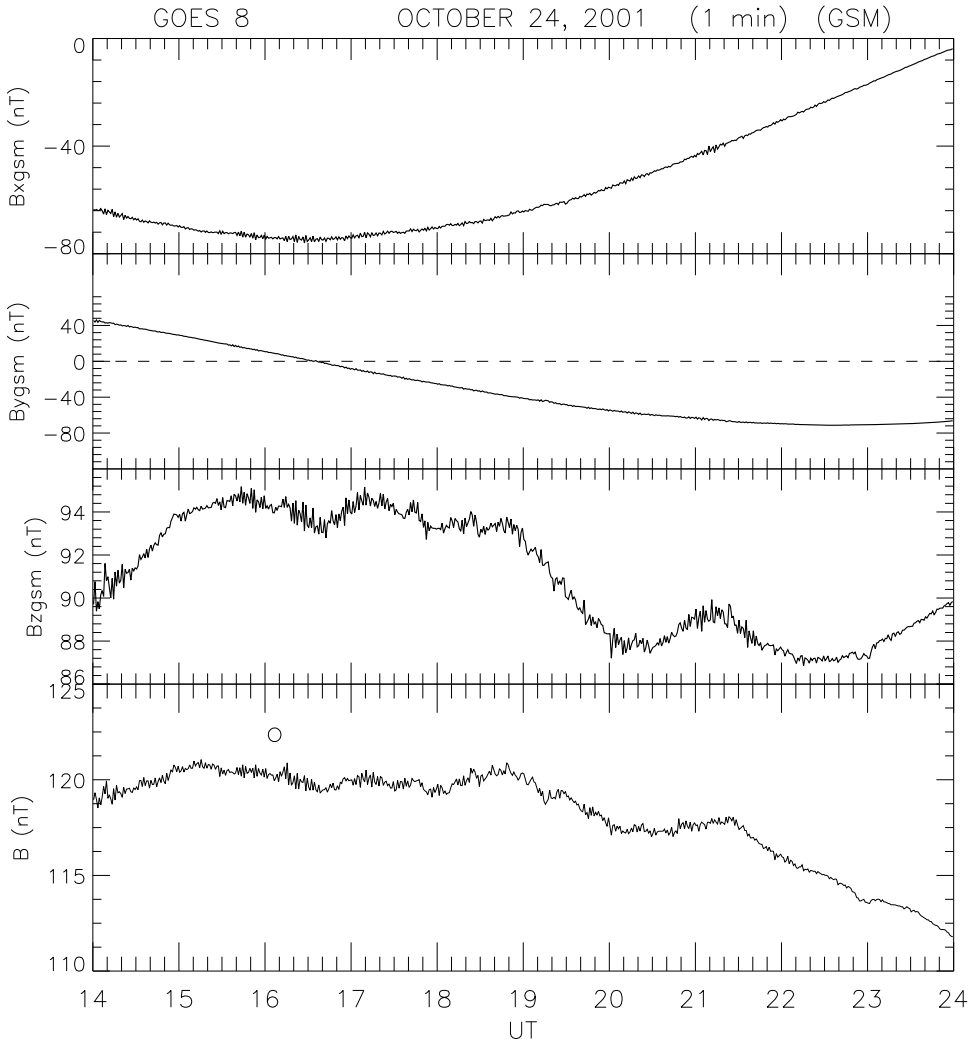

Figure 15. Components of the geomagnetic field at geostationary heights measured by GOES 8 for the interval 14–24 UT (06–18 MLT) in GSM. The circled symbol in the last panel indicates local magnetic noon.

investigate. In view of these sources of discrepancies, agreement between theory and observations is to be understood only in a time-averaged sense.

[33] We have postulated that the cause of the pulsed accelerated flows at Wind is waves which make the boundary layer oscillate so that the spacecraft encounters magnetopause ripples as they sweep past it. Their generating mechanism is unclear. We speculated that they might be caused by the Kelvin-Helmholtz instability and we preferred the inner edge of the boundary layer to the magnetopause itself, partly because the former has less magnetic shear across it, and partly because they appear as soon as Wind enters the LLBL.

[34] There are other possible alternative explanations of the accelerated bursts of plasma. We consider these next. One is suggested by the average frequency at which they recur, 3.2 mHz. This is of interest because 3.3 mHz is an oft-quoted frequency inherent to the solar wind. Indeed, in a recent paper, *Viall et al.* [2009] show that the frequency 3.3 mHz is one that shows up more often than others in the solar wind. In this regard it has also been postulated in the past that some ULF pulsations in the dayside magnetosphere are directly driven at the intrinsic solar wind frequencies.

[35] To check the latter, we examined 1-min GOES 8 data from 10–22 UT (from NASA's cdaweb site), corresponding to 06–18 MLT. The time series is shown in Figure 15. The circled symbol in the last panel marks local magnetic noon, so these are dayside observations. Indeed, a fluctuation in B_z is very evident. Performing a spectral analysis we find in Figure 16 that the corresponding frequency is ~7.0 mHz (period 2.38 min). The mismatch between this frequency and that in the LLBL makes it unlikely that the pulsations at Wind are an eigenfrequency of the magnetosphere being directly driven by an intrinsic frequency of the solar wind.

[36] Another possible explanation is that the LLBL pulses are similar to those induced in the magnetosheath by the passage of an ICME. Thus *Lavraud et al.* [2007] showed a clear case of an accelerated flow region in the magnetosheath and argued compellingly that it is not of reconnection origin but due rather to the low Alfvén Mach number and the action of strong magnetic tension and pressure gradient forces. (We note that an even earlier

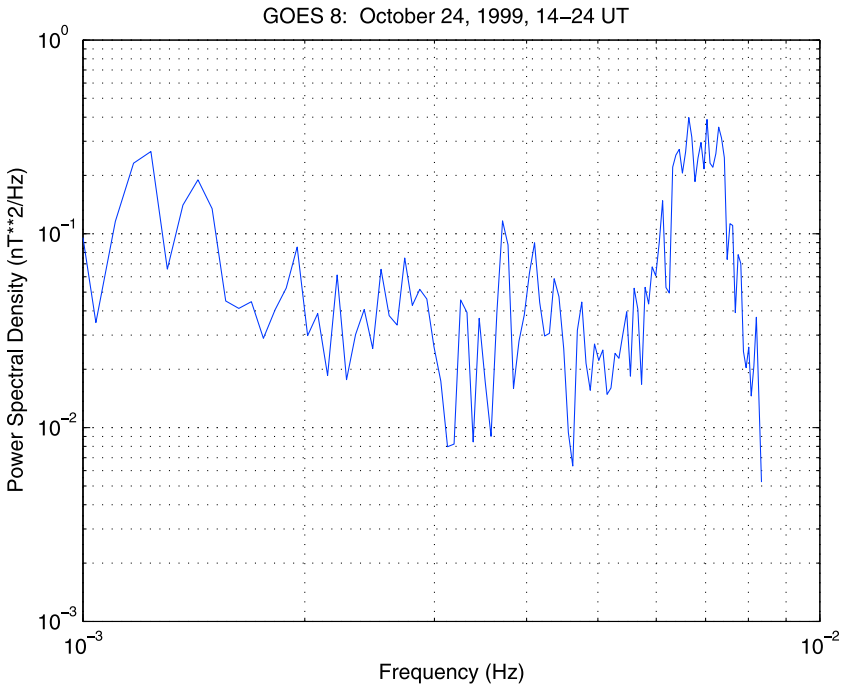

Figure 16. The power spectral density of the B_z component at Goes 8.

example of flows in the magnetosheath much larger than in the solar wind in Geotail data was reported by *Petrinec et al.* [1997].) They studied Cluster data during Earth passage of an ICME on November 25, 2001. The accelerations exceeded by 100's of km s^{-1} the speed of the solar wind (as in our case). The locations of the observing spacecraft, too, are comparable: both were tailward of terminator with Cluster at dusk (−3.4, 18.0, −5.2) Re, as opposed to Wind at dawn. The Alfvén Mach number, a key parameter controlling magnetosheath behavior [*Farrugia et al.*, 1995; *Lavraud et al.*, 2007; *Lavraud and Borovsky*, 2008] was low and of order 2. The interplanetary field was strongly northward pointing. By contrast, in our case Wind is making observations in boundary layer; bursts of strong flows were seen; the magnetic field was dominated by B_x; and the Alfvén Mach number is not so small (~6 in Figure 3, and more if we include the alpha-particle contribution to the density). Therefore we do not believe that this is a viable explanation for the present observations.

[37] A further possibility is that the almost-periodic pulsations originate at the bow shock, particularly near the subsolar point, where the bow shock is a quasi-parallel shock and where the streamlines pass close to the magnetopause. Reformation of the quasi-parallel shock caused by so-called SLAMs (Short Large Amplitude Magnetic Structures; *Schwartz and Burgess* [1991], *Burgess et al.* [2005]) may generate pulsations that may propagate to large distances. However, these events do not usually occur periodically. Waves produced in the shock layer are of higher frequency and they are usually efficiently damped downstream of the shock [*Scholer and Kucharek*, 1999]. So quasi-parallel shock reformation processes seem unlikely, but they cannot be excluded entirely.

[38] The frequency of occurrence of a few minutes suggests a last possibility, bursty reconnection (Flux transfer events, FTEs). From statistical analysis, the recurrence rate of FTEs is 6–8 min [*Rijnbeek et al.*, 1984; *Berchem and Russell*, 1984]. This is somewhat longer than what we observe. Further, the strict periodicity in a reconnection process is unexpected. Finally, bearing in mind (i) the non-synchronous arrival of high speeds and high densities; and (ii) the sharp changes on one side of each pulse, make a bursty reconnection interpretation improbable.

[39] The data we studied has a lesson to impart. They show that even in a very "benign" interplanetary situation, the magnetosheath is prone to internal instabilities, turbulence and motion of boundaries which make the real situation more complicated to handle.

Appendix A

[40] Linear magnetic perturbations are determined by equations

$$\nabla \cdot \mathbf{B} = 0, \tag{A1}$$

$$\nabla \times (\mathbf{V} \times \mathbf{B}) = 0, \tag{A2}$$

where the plasma velocity is assumed to satisfy the continuity equation

$$\nabla \cdot (\rho \mathbf{V}) = 0. \tag{A3}$$

[41] Each streamline can be parameterized by two quantities α and β which retain constant values along a given line and which function as Euler potentials of the velocity field.

For the uniform flow upstream of the bow shock, streamlines are assumed to be parallel to the x axis, and the quantities α and β are set to be equal to the coordinates z and y, respectively. In addition the quantities α and β, we introduce a third quantity γ, which times the motion of a test particle along a given streamline. As follows from the definitions above, these three quantities satisfy the equations

$$\mathbf{V}\cdot\nabla\alpha = 0, \quad \mathbf{V}\cdot\nabla\beta = 0, \quad \mathbf{V}\cdot\nabla\gamma = V_\infty. \tag{A4}$$

[42] Considering the system (A4) as algebraic linear equations with respect to the velocity components V_x, V_y, V_z, we find

$$\mathbf{V} = \frac{V_\infty}{I}\nabla\alpha\times\nabla\beta, \tag{A5}$$

where I is the Jacobian

$$I = \frac{D(\alpha,\beta,\gamma)}{D(x,y,z)}. \tag{A6}$$

Inserting (A5) into the mass conservation equation $\nabla\cdot(\rho\mathbf{V}) = 0$, we find

$$I = \rho/(\rho_\infty). \tag{A7}$$

Finally, equation (A5) yields

$$\rho\mathbf{V} = \rho_\infty V_\infty\nabla\alpha\times\nabla\beta. \tag{A8}$$

[43] A general solution of the linear equations with respect to the magnetic field components is given by

$$\mathbf{B} = C_1\nabla\alpha\times\nabla\beta + C_2\nabla\beta\times\nabla\gamma + C_3\nabla\gamma\times\nabla\alpha. \tag{A9}$$

Here coefficients C_1, C_2 and C_3 are to be determined from the input conditions for IMF components in the solar wind upstream of the bow shock, where we have

$$\alpha = z, \quad \beta = y, \quad \gamma = -x + const, \qquad \mathbf{B} = (B_{x\infty},\ B_{y\infty},\ B_{z\infty}). \tag{A10}$$

[44] Using conditions (A10), we obtain a formula for the magnetic vector in the magnetosheath

$$\mathbf{B} = -B_{x\infty}\rho\mathbf{V}/(\rho_\infty V_\infty) + B_{z\infty}\nabla\beta\times\nabla\gamma + B_{y\infty}\nabla\gamma\times\nabla\alpha. \tag{A11}$$

The final step is to determine analytical expressions for the α, β, γ.

[45] For axisymmetrical flow, functions α and β can be expressed via the stream function ψ

$$\alpha = \sqrt{2\psi}\cos(\phi), \qquad \beta = \sqrt{2\psi}\sin(\phi). \tag{A12}$$

[46] Inserting (A12) into equations (A11), we find

$$B_\phi = [-B_{z\infty}\sin(\phi) + B_{y\infty}\cos(\phi)]\frac{\tilde{r}\tilde{\rho}}{\sqrt{2\psi}}, \tag{A13}$$

$$B_l = -[B_{z\infty}\cos(\phi) + B_{y\infty}\sin(\phi)]\sqrt{2\psi}\frac{1}{\tilde{r}}\frac{\partial\gamma}{\partial\mu} - B_{x\infty}\tilde{\rho}\tilde{V}_l, \tag{A14}$$

$$B_\mu = [B_{z\infty}\cos(\phi) + B_{y\infty}\sin(\phi)]\sqrt{2\psi}\frac{1}{\tilde{r}}\frac{\partial\gamma}{\partial l} - B_{x\infty}\tilde{\rho}\tilde{V}_\mu. \tag{A15}$$

Here subscripts l, ϕ and μ denote the meridional, azimuthal and normal components with respect to the magnetopause. The dimensionless gasdynamic quantities are defined as

$$\tilde{V}_{l,\mu} = V_{l,\mu}/V_\infty, \quad \tilde{\rho} = \rho/\rho_\infty, \quad \tilde{r} = r/R_0, \tag{A16}$$

where r is the distance to the axis of symmetry x, and R_0 is the subsolar radius of the magnetopause. The equation for γ can be simplified near the streamlined surface by expanding $\tilde{V}_\mu$ in a Taylor series with respect to the normal distance to the magnetopause

$$\tilde{V}_l\frac{\partial\gamma}{\partial l} - \mu\, a(l)\frac{\partial\gamma}{\partial\mu} = 1. \tag{A17}$$

Here l is the meridional distance from the stagnation point along the surface. The solution of this equation is

$$\gamma = \left[-\frac{1}{a_0}\ln(\mu) + \int_0^l (1 - a/a_0)\frac{dl}{\tilde{V}_l}\right]. \tag{A18}$$

Near the streamlined surface we have the Taylor expansion of the stream function

$$\psi = \rho\tilde{V}_l\tilde{r}\mu. \tag{A19}$$

[47] Using (A18) and (A19) we derive simplified analytical formulae for the magnetic field components near the magnetopause

$$B_l = -[B_{z\infty}\cos(\phi) + B_{y\infty}\sin(\phi)]\cdot\left(\frac{2\tilde{\rho}\tilde{V}_l}{\tilde{r}\mu}\right)^{1/2}\frac{1}{a_0} - B_{x\infty}\tilde{\rho}\tilde{V}_l, \tag{A20}$$

$$B_\phi = [-B_{z\infty}\sin(\phi) + B_{y\infty}\cos(\phi)]\left(\frac{\tilde{r}\tilde{\rho}}{2\tilde{V}_l\mu}\right)^{1/2}, \tag{A21}$$

$$B_\mu = [B_{z\infty}\cos(\phi) + B_{y\infty}\sin(\phi)]\cdot\left(\frac{2\tilde{\rho}\mu}{\tilde{V}_l\tilde{r}}\right)^{1/2}\frac{(a_0 - a)}{a_0} - B_{x\infty}\tilde{\rho}\tilde{V}_\mu. \tag{A22}$$

The applicability of these equations (A20)–(A22) is constrained by condition $\mu \geq \delta_m/R_0$, where δ_m is the thickness of the magnetopause and where they exhibit a singularity.

Appendix B: Analytical Estimation of the Gas Dynamic Parameters in the Magnetosheath for Quasi-Aligned Fields

[48] For a steady ideal MHD flow where the velocity and magnetic fields are (anti)parallel, the energy and mass conservation equations yield the Bernoulli equation

$$\frac{1}{2}V^2 + \frac{\kappa}{\kappa-1}\frac{P}{\rho} = \frac{1}{2}V_\infty^2 + \frac{\kappa}{\kappa-1}\frac{P_\infty}{\rho_\infty}, \tag{B1}$$

where κ is the polytropic index, assumed here = 5/3.

[49] In addition, we use an adiabatic equation along a flow streamline

$$\frac{P}{\rho^{5/3}} = A = const. \tag{B2}$$

For the pressure along the magnetopause surface we apply the well-known Newtonian relation

$$P = K\rho_\infty V_\infty^2 \cos^2(\theta), \tag{B3}$$

[e.g., see *Spreiter et al.*, 1966; *Petrinec and Russell*, 1997] where θ is the angle between the outward normal to the magnetopause and the free-stream velocity vector V_∞, K is a constant equal to 0.88 for high Mach number [*Spreiter and Rizzi*, 1974].

[50] Using now equations (B1), (B2), (B3), we determine the velocity and plasma density as function of distance along the magnetopause

$$V(r) = V_\infty\left\{1 + 5\left[\frac{P_\infty}{\rho_\infty V_\infty^2} - K\left(\frac{\rho_\infty}{\rho_0}\right)\cos(\theta)^{0.8}\right]\right\}^{1/2}, \tag{B4}$$

$$\rho = \rho_0 \cos(\theta)^{6/5}, \tag{B5}$$

where the quantity ρ_0 can be determined from the condition that the velocity = 0 at the stagnation point

$$\rho_0 = \frac{5K\rho_\infty}{1 + 5\frac{P_\infty}{\rho_\infty V_\infty^2}}. \tag{B6}$$

Formulae (B4) and (B5) allow us to estimate the plasma velocity and density near the magnetopause.

[51] As one can see by *Spreiter and Rizzi* [1974], the plasma velocity has a small variation across the magnetosheath at the flanks. The plasma density has a monotonic variation (approximately linear) between the magnetopause and the bow shock. We assume a linear dependence

$$\rho(\mu) = \rho_0 + \frac{(\rho_s - \rho_0)}{\Delta}\mu, \tag{B7}$$

where ρ_s is the plasma density just downstream of the bow shock, Δ is the distance between the bow shock and the magnetopause. The stream function across the magnetosheath can be found as integral

$$\psi(\mu, r) = \int_0^\mu \tilde{\rho}\,\tilde{V}_l\,\tilde{r}\,d\mu. \tag{B8}$$

This stream function vanishes at the magnetopause, and it increases monotonically across the magnetosheath towards the bow shock.

[52] **Acknowledgments.** The authors would like to thank David Burgess for helpful discussions. Part of this work was done when NVE was on a research visit to the Space Science Center of the University of New Hampshire, USA. This work is supported by NASA grants NNX08AD11G and NNG06GD41G, and also by RFBR grants 07-05-00135, 09-05-91000-ANF_a and by Program 16 of RAS. R. P. Lin has been supported in part by NASA grant NNX08AE34G at UC Berkeley, and the WCU grant (R31-10016) funded by the Korean Ministry of Education, Science and Technology. We thank D. J. McComas and H. J. Singer for the ACE plasma data and GOES magnetic field data, respectively, obtained through NASA cdaweb site.

[53] Masaki Fujimoto thanks Steven Petrinec and another reviewer for their assistance in evaluating this paper.

References

Anderson, B. J. (1995), ULF signals observed near the magnetopause, in *Physics of the Magnetopause*, *AGU Monogr. Ser*, vol. 90, edited by P. Song, B. U. Ö. Sonnerup, and M. F. Thomsen, pp. 269–276, AGU, Washington, D. C.

Berchem, J., and C. T. Russell (1984), Flux transfer events on the magnetopause: Spatial distribution and controlling factors, *J. Geophys. Res.*, *89* (A8), 6689–6703, doi:10.1029/JA089iA08p06689.

Burgess, D., et al. (2005), Quasi-parallel shock structure and processes, *Space Sci. Rev.*, *118*, 205–222.

Burlaga, L. F., S. P. Plunkett, and P.-C. StCyr (2002), Successive CMEs and complex ejecta, *J. Geophys. Res.*, *107*(A10), 1266, doi:10.1029/2001JA000255.

Erkaev, N. V. (1988), Results of the investigation of MHD flow around the magnetosphere, *Geomagn. Aeron.*, *28*, 455–464.

Farrugia, C. J., N. V. Erkaev, H. K. Biernat, and L. F. Burlaga (1995), Anomalous magnetosheath properties during Earth passage of an interplanetary magnetic cloud, *J. Geophys. Res.*, *100*, 19,245–19,257, doi:10.1029/95JA01080.

Farrugia, C. J., A. Grocott, P. E. Sandholt, S. W. H. Cowley, Y. Miyoshi, F. J. Rich, V. K. Jordanova, R. B. Torbert, and A. Sharma (2007), The magnetosphere under weak solar wind forcing, *Ann. Geophys.*, *25*, 1–15.

Gopalswamy, N., S. Yashiro, M. L. Kaiser, R. A. Howard, and J.-L. Bougeret (2001), Radio signatures of coronal mass ejection interaction: Coronal mass ejection cannibalism?, *Astrophys. J.*, *548*, L91–L94.

Imai, I. (1960), On flows of conducting fluids past bodies, *Rev. Mod. Phys.*, *32*, 992–999.

Lavraud, B., and J. E. Borovsky (2008), Altered solar wind-magnetosphere interaction at low Mach numbers: Coronal mass ejections, *J. Geophys. Res.*, *113*, A00B08, doi:10.1029/2008JA013192.

Lavraud, B., J. E. Borovsky, A. J. Ridley, E. W. Pogue, M. F. Thomsen, H. Rème, A. N. Fazakerly, and E. A. Lucek (2007), Strong bulk plasma acceleration in Earth's magnetosheath: A magnetic slingshot effect?, *Geophys. Res. Lett.*, *34*, L14102, doi:10.1029/2007GL030024.

Lees, L. (1964), Interaction between the solar wind plasma and the geomagnetic cavity, *AIAA J.*, *2*, 1576–1582.

Lepping, R. P., et al. (1995), The Wind magnetic field investigation, *Space Sci. Rev.*, *71*, 207–229.

Lin, R. P., et al. (1995), A three-dimensional plasma and energetic particle investigation for the Wind spacecraft, *Space Sci. Revs.*, *71*, 125–153.

Lopez, R. E. (1987), Solar cycle invariance in solar wind proton temperature relationships, *J. Geophys. Res.*, *92*, 11,187–11,194.

Merka, J., A. Szabo, J. Safranková, and Z. Nemecek (2003), Earth's bow shock and magnetopause in the case of a field-aligned upstream flow: Observation and model comparison, *J. Geophys. Res.*, *108*(A7), 1269, doi:10.1029/2002JA009697.

Petrinec, S. M., and C. T. Russell (1997), Investigations of hydrodynamic and magnetohydrodynamic equations across the bow shock and along the outer edge of planetary obstacles, *Adv. Space Sci.*, *20*(4–5), 743–746.

Petrinec, S. M., T. Mukai, A. Nishida, T. Yamamoto, T. K. Nakamura, and S. Kokubun (1997) Geotail observations of magnetosheath flow near the

magnetopause, using Wind as a solar wind monitor, *J. Geophys. Res.*, *102*, 26,943–26,959.
Pudovkin, M. I., and V. S. Semenov (1977), Stationary frozen-in coordinate system, *Ann. Geophys.*, *33*, 429–433.
Rijnbeek, R. P., S. W. H. Cowley, D. J. Southwood, and C. T. Russell (1984), A survey of dayside flux transfer events observed by ISEE 1 and 2 magnetometers, *J. Geophys. Res.*, *89*(A2), 786–800.
Sahraoui, F., G. Belmont, L. Rezeau, and N. Corniieau-Wehrlin (2006), Anisotropic turbulent spectra in the terrestrial magnetosheath as seen by the Cluster spacecraft, *Phys. Res. Lett.*, *96*, 075002.
Scholer, M., and H. Kucharek (1999), Quasi-parallel collisionless shocks, *Astrophys. Space Sci.*, *263*, 527–543.
Schwartz, S. J., and D. Burgess (1991), Quasi-parallel shocks: A patchwork of three-dimensional structures, *Geophys. Res. Lett.*, *18*, 373–376, doi:10.1029/91GL00138.
Shue, J.-H., et al. (1998), Magnetopause location under extreme solar wind conditions, *J. Geophys. Res.*, *103*, 17,691–17,700, doi:10.1029/98JA01103.
Shue, J.-H., J.-K. Chao, J. P. McFadden, A. Suvorova, V. Angelopoulos, K. H. Glassmeier, and F. Plaschke (2009), Anomalous magnetosheath flows and distorted subsolar magnetopause for radial interplanetary magnetic fields, *Geophys. Res. Lett.*, *36*, L18112, doi:10.1029/2009GL039842.
Siscoe, G. (2002), Footnotes to Spreiter, *Planet. Space Sci.*, *50*, 443–446.
Sonnerup, B. U. Ö. (1974), The reconnecting magnetopause, in *Magnetospheric Physics*, edited by B. M. McCormac, pp. 23–33, D. Reidel, Norwell, Mass.
Spreiter, J. R., and A. Y. Alksne (1969), Plasma flow around the magnetosphere, *Rev. Geophys.*, *7*, 11–50, doi:10.1029/RG007i001p00011.
Spreiter, J. R., and A. W. Rizzi (1974), Aligned magnetohydrodynamic solution for solar wind flow past the earth's magnetosphere, *Acta Astron.*, *1*, 15–35.
Spreiter, J. R., and S. Stahara (1980), A new predictive model for determining solar wind-terrestrial planet interaction, *J. Geophys. Res.*, *85*, 6769–6777.
Spreiter, J. R., A. L. Summers, and A. Y. Alksne (1966), Hydromagnetic flow around the magnetosphere, *Planet. Space Sci.*, *14*, 223–253.
Steinberg, J. T., A. J. Lazarus, K. W. Ogilvie, R. Lepping, and J. Byrnes (1996), Differential flow between solar wind protons and alpha particles: First WIND observations, *Geophys. Res. lett.*, *23*, 1183–1186, doi:10.1029/96GL00628.
Viall, N. M., L. Kepko, and H. E. Spence (2009), Relative occurrence rates and connection of discrete frequency oscillations in the solar wind density and dayside magnetosphere, *J. Geophys. Res.*, *114*, A01201, doi:10.1029/2008JA013334.
Zwan, B. J., and R. A. Wolf (1976), Depletion of the solar wind plasma near a planetary boundary, *J. Geophys. Res.*, *81*, 1636–1648.

H. K. Biernat, Space Research Institute, Austrian Academy of Sciences, Schmiedlstr. 6, Graz A-8042, Austria.
N. V. Erkaev, Institute for Computational Modeling, Russian Academy of Sciences, Academgorodok 50/44, Krasnoyarsk 660036, Russia.
C. J. Farrugia, H. Kucharek, H. Matsui, C. W. Smith, and R. B. Torbert, Space Science Center and Department of Physics, University of New Hampshire, 39 College Rd., Durham, NH 03824, USA. (charlie.farrugia@unh.edu)
F. T. Gratton, Instituto de Física del Plasma, Consejo Nacional de Investigaciones Científicas y Técnicas, Buenos Aires, Argentina.
R. P. Lepping, K. W. Ogilvie, and A. Szabo, Space Weather Laboratory, NASA Goddard Space Flight Center, Code 674, Building 21, Room 228, Greenbelt, MD 20771, USA.
R. P. Lin, Space Sciences Laboratory, University of California, 7 Gauss Way, Berkeley, CA 94720, USA.